Ab initio calculation of spin fluctuation spectra using time-dependent density functional perturbation theory, plane waves, and pseudopotentials

Kun Cao,[1] Henry Lambert,[1,*] Paolo G. Radaelli,[2] and Feliciano Giustino[1]
[1]*Department of Materials, University of Oxford, Parks Road, Oxford OX1 3PH, United Kingdom*
[2]*Clarendon Laboratory, Department of Physics, University of Oxford, Parks Road, Oxford OX1 3PU, United Kingdom*

(Received 19 July 2017; revised manuscript received 11 November 2017; published 19 January 2018)

We present an implementation of time-dependent density functional perturbation theory for spin fluctuations, based on plane waves and pseudopotentials. We compute the dynamic spin susceptibility self-consistently by solving the time-dependent Sternheimer equation, within the adiabatic local density approximation to the exchange and correlation kernel. We demonstrate our implementation by calculating the spin susceptibility of representative elemental transition metals, namely bcc Fe, fcc Ni, and bcc Cr. The calculated magnon dispersion relations of Fe and Ni are in agreement with previous work. The calculated spin susceptibility of Cr exhibits a soft-paramagnon instability, indicating the tendency of the Cr spins to condense in an incommensurate spin density wave phase, in agreement with experiment.

DOI: 10.1103/PhysRevB.97.024420

I. INTRODUCTION

Spin fluctuations play a central role in magnetic systems [1]. For example they underpin fundamental thermodynamic properties of magnets, such as the Curie temperature and the heat capacity; they have long been discussed as a potential source of pairing in high-temperature superconductivity [2,3]; and they offer new opportunities in the development of spintronics [4–6] and multiferroics [7].

In ordered magnets, spin fluctuations manifest themselves in two forms, magnons and Stoner excitations [1,8]. In standard textbooks, magnons or 'spin waves' are typically illustrated as a collective, wavelike rotation of spins around their direction in the ground state [9]; Stoner or 'spin flip' excitations correspond instead to electronic transitions from occupied to empty states, whereby the electron spin is reversed; this process can alternatively be described as the creation of an electron-hole singlet pair of spins. When spin waves and spin flip excitations are degenerate, the spin wave is attenuated and sharp magnon excitations cease to exist. This phenomenon is referred to as Landau damping [10], and a clear discussion for the simplified case of the uniform electron gas can be found in Refs. [1,11]. Landau damping is usually important in metallic systems [12], while it is generally weak in insulators, owing to the large energy needed to excite Stoner pairs across the band gap.

The majority of studies on spin waves are currently based on the adiabatic approximation, whereby spin and electronic excitations are decoupled [13,14]. In this approach one maps the magnetic degrees of freedom into an array of local spins and determines the coupling parameters from total energy calculations based on density functional theory (DFT), or from experiments. This approach proved to work well for insulating magnets, but carries some limitations. For example the adiabatic approximation does not admit Stoner excitations, therefore Landau damping is not captured, and the magnon energy renormalization resulting from Stoner excitations is absent [11,12,15]. In addition this approach is sensitive to the choice of the discrete spin model and the determination of its parameters. It is clear that a more general approach is desirable in this context, thus motivating the need for a fully *ab initio* approach to spin waves.

The central quantity to describe spin fluctuations is the wave-vector- ($\mathbf{q}$) and energy- (ω) dependent spin susceptibility, $\chi(\mathbf{q},\omega)$ (in the following Hartree atomic units will be assumed). Magnon excitations correspond to the poles of $\chi(\mathbf{q},\omega)$ [1]. A promising approach for calculating $\chi(\mathbf{q},\omega)$ from first principles is given by time-dependent density functional perturbation theory (TD-DFPT) [16]. The main appeal of this method is that it allows one to describe spin waves and Stoner excitations on the same footing, without invoking materials-specific approximations. TD-DFPT for spin fluctuations has already been demonstrated using either all-electron [15,17] or pseudopotential [18] implementations. Using the adiabatic local density approximation (ALDA) to the exchange and correlation kernel [16,19–21], it was shown that the formalism can capture the experimental magnon spectra of typical transition metals (Fe, Co, Ni, Cr) with reasonable accuracy [15,17,18], provided the underlying DFT calculations could reproduce measured Stoner splittings.

Given these encouraging results on the use of TD-DFPT for calculating spin fluctuations, it would be desirable to have these techniques available in the context of popular DFT implementations based on plane waves and pseudopotentials. The first implementation of this type was reported not long ago [18]. In this implementation the authors calculated the spin susceptibility using the sum-over-states approach, and dealt with Brillouin zone sampling using maximally-localized Wannier functions [22].

In this work we present a plane waves/pseudopotential implementation of TD-DFPT for spin fluctuations which does

*Present address: Physics Department, King's College, London, United Kingdom.

not rely on unoccupied electronic states. Our implementation employs the time-dependent Sternheimer equation, in the spirit of related work in the area of GW calculations [23–29]. The implementation is based on the linear-response modules of the QUANTUM ESPRESSO materials simulation suite [30] and is currently hosted on our GitHub repository [31]. We demonstrate this development by calculating the spin fluctuations spectra of bcc iron, fcc nickel, and bcc chromium. Our results are in good agreement with previous calculations. The calculated spectra of Fe and Cr are in agreement with experiment, while our results for Ni deviate from experiments owing to the incorrect Stoner splitting in the underlying DFT calculation.

The paper is organized as follows. In Sec. II we present the TD-DFPT formalism for the spin susceptibility and the time-dependent Sternheimer equation. We also discuss how to treat fractional occupations in metals and how to perform the symmetry-reduction of the Brillouin zone. At the end of this section we provide some technical details of the implementation. In Sec. III we present calculation results on the elemental transition metals Fe, Ni, and Cr. Here we compare our results to previous calculations as well as experiments. We offer our conclusions in Sec. IV, together with an outlook on future work.

II. SPIN SUSCEPTIBILITY IN TIME-DEPENDENT DENSITY FUNCTIONAL PERTURBATION THEORY

A. General theory

In this section we summarize the generalization of the TD-DFPT formalism [16] to noncollinear spins, as already discussed in Refs. [15,17,18,32,33]. In the following we do not consider spin-orbit coupling, and we use the spin g factor $g = 2$. The DFT Kohn-Sham equations for a noncollinear spin system read:

$$\left[-\frac{\nabla^2}{2}\hat{I} + \hat{V}_{\rm scf}(\mathbf{r})\right]\vec{\psi}_{n\mathbf{k}}(\mathbf{r}) = \epsilon_{n\mathbf{k}}\vec{\psi}_{n\mathbf{k}}(\mathbf{r}), \tag{1}$$

where $\hat{I}$ is the 2×2 identity matrix, and $\hat{V}_{\rm scf}$ is the Kohn-Sham potential, expressed as the following 2×2 matrix:

$$\hat{V}_{\rm scf}(\mathbf{r}) = V_{\rm scf}(\mathbf{r})\hat{I} + \boldsymbol{\sigma}\cdot\mathbf{B}_{\rm scf}(\mathbf{r}). \tag{2}$$

In this expression $V_{\rm scf}$ is the scalar part of the self-consistent potential, and $\mathbf{B}_{\rm scf}$ is the effective magnetic field arising from external potential as well as exchange and correlation [34]. The Pauli matrix is given by $\boldsymbol{\sigma} = \sigma^1\mathbf{u}_x + \sigma^2\mathbf{u}_y + \sigma^3\mathbf{u}_z$, with σ^i the usual 2×2 Pauli matrices, and the unit vectors such as $\mathbf{u}_x$ denoting Cartesian directions. $\vec{\psi}_{n\mathbf{k}}$ is a Kohn-Sham two-spinor eigenfunction with wave vector $\mathbf{k}$, band index n, and energy $\epsilon_{n\mathbf{k}}$, and corresponds to two scalar functions dependent on the space coordinate $\mathbf{r}$, as follows:

$$\vec{\psi}_{n\mathbf{k}}(\mathbf{r}) = \begin{bmatrix}\psi^1_{n\mathbf{k}}(\mathbf{r})\\ \psi^2_{n\mathbf{k}}(\mathbf{r})\end{bmatrix}. \tag{3}$$

Using this notation, the 2×2 density matrix becomes:

$$\rho_{\alpha\beta}(\mathbf{r}) = \frac{1}{N_{\mathbf{k}}}\sum_{\mathbf{k},n\in{\rm occ}}\psi^{\alpha,*}_{n\mathbf{k}}(\mathbf{r})\,\psi^{\beta}_{n\mathbf{k}}(\mathbf{r}), \quad \alpha,\beta = 1,2, \tag{4}$$

where $N_{\mathbf{k}}$ is the number of $\mathbf{k}$ points used to discretize the first Brillouin zone (we assume a uniform sampling), and the asterisk denotes complex conjugation. Using the Pauli matrix $\boldsymbol{\sigma}$, the density matrix can be decomposed as in Eq. (2):

$$\hat{\rho}(\mathbf{r}) = \tfrac{1}{2}[n(\mathbf{r})\hat{I} + \boldsymbol{\sigma}\cdot\mathbf{m}(\mathbf{r})], \tag{5}$$

where $n(\mathbf{r})$ is the standard electron charge density, and $\mathbf{m}(\mathbf{r})$ is the electron spin density.

In order to facilitate the algebra it is convenient to introduce an alternative expression for the density matrix, using vector notation:

$$\rho^0 = n,\ \rho^1 = m_x,\ \rho^2 = m_y,\ \rho^3 = m_z. \tag{6}$$

Using these definitions, together with $\sigma^0 = \hat{I}$ we can rewrite Eq. (4) as follows:

$$\rho^i(\mathbf{r}) = \frac{1}{N_{\mathbf{k}}}\sum_{\mathbf{k},n\in{\rm occ}}\vec{\psi}_{n\mathbf{k}}(\mathbf{r})^\dagger\,\sigma^i\,\vec{\psi}_{n\mathbf{k}}(\mathbf{r}), \quad i = 0,\ldots 3, \tag{7}$$

where the dagger indicates the Hermitian conjugate.

We now consider a time-dependent external perturbation, which can be either an electric potential or a magnetic field, $\delta V^i_{\rm ext}(\mathbf{r}t)$, with:

$$\delta V^0_{\rm ext}(\mathbf{r}t) = V_{\rm ext}(\mathbf{r}t), \quad \delta V^1_{\rm ext}(\mathbf{r}t) = B^x_{\rm ext}(\mathbf{r}t), \tag{8}$$

and similarly for $j = 2,3$. We neglect diamagnetic effects, so that the magnetic field $\mathbf{B}_{\rm ext}$ only couples to the spin degrees of freedom. In linear-response theory the variation of the density matrix in response to the external perturbation is written as:

$$\delta\rho^i(\mathbf{r}t) = \sum_j\int d(\mathbf{r}'t')\,\chi^{ij}(\mathbf{r}t,\mathbf{r}'t')\,\delta V^j_{\rm ext}(\mathbf{r}'t'), \tag{9}$$

where the sum runs over the components of the four vector, and $\chi^{ij}(\mathbf{r}t,\mathbf{r}'t')$ is the generalized susceptibility. In TD-DFPT the generalized susceptibility is formally obtained via a Dyson's equation [16]:

$$\begin{aligned}\chi^{ij}&(\mathbf{r}t,\mathbf{r}'t')\\ &= \chi^{ij}_{\rm KS}(\mathbf{r}t,\mathbf{r}'t') + \sum_{kl}\int d(\mathbf{r}_1t_1)d(\mathbf{r}_2t_2)\\ &\quad\times\chi^{ik}_{\rm KS}(\mathbf{r}t,\mathbf{r}_1t_1)\left[f^{kl}_{xc}(\mathbf{r}_1t_1,\mathbf{r}_2t_2) + \frac{2\delta_{k0}\delta_{l0}\delta(t_1-t_2)}{|\mathbf{r}_1-\mathbf{r}_2|}\right]\\ &\quad\times\chi^{lj}(\mathbf{r}_2t_2,\mathbf{r}'t'),\end{aligned} \tag{10}$$

where f^{kl}_{xc} is the exchange and correlation kernel, and $\chi^{ij}_{\rm KS}$ is the noninteracting Kohn-Sham susceptibility.

The exchange-correlation kernel is usually written within the adiabatic local spin-density approximation (ALSDA) to time-dependent DFT, meaning that one uses the static LSDA kernel at equal times [15,16,20,21]:

$$f^{ij}_{xc}(\mathbf{r}t,\mathbf{r}'t') = \frac{\delta^2E_{xc}}{\delta\rho^i(\mathbf{r})\rho^j(\mathbf{r}')}\delta(\mathbf{r}-\mathbf{r}')\delta(t-t'). \tag{11}$$

We note that this choice carries the additional implicit approximation that the ALSDA kernel is derived by considering an electron gas with collinear spins.

The Kohn-Sham susceptibility appearing in Eq. (10) is defined so as to yield the density-matrix response to a variation of the self-consistent potential, in analogy with Eq. (9):

$$\delta\rho^i(\mathbf{r}t) = \sum_j\int d(\mathbf{r}'t')\,\chi^{ij}_{\rm KS}(\mathbf{r}t,\mathbf{r}'t')\,\delta V^j_{\rm scf}(\mathbf{r}'t'). \tag{12}$$

In view of practical calculations it is more convenient to work in the frequency domain rather than in the time domain. Since the unperturbed Hamiltonian is time independent, the susceptibility depends only on the time difference $t - t'$. As a result, the last equation can be rewritten in the frequency domain as follows:

$$\delta\rho^i(\mathbf{r},\omega) = \sum_j \int d\mathbf{r}'\, \chi^{ij}_{\rm KS}(\mathbf{r},\mathbf{r}',\omega)\, \delta V^j_{\rm scf}(\mathbf{r}',\omega), \tag{13}$$

having defined:

$$\delta\rho^i(\mathbf{r},\omega) = \int dt\, \delta\rho^i(\mathbf{r}t)\, e^{-i\omega t}, \tag{14}$$

and similarly for $\delta V^i_{\rm scf}(\mathbf{r},\omega)$ and $\chi^{ij}_{\rm KS}(\mathbf{r},\mathbf{r}',\omega)$. Equations (9)–(11) are transformed into the frequency domain along the same lines. Using standard perturbation theory, the Kohn-Sham susceptibility in the frequency domain can now be written explicitly in terms of unperturbed Kohn-Sham spinors [16]:

$$\chi^{ij}_{\rm KS}(\mathbf{r},\mathbf{r}',\omega) = \frac{1}{N_{\mathbf{k}}^2} \sum_{nm,\mathbf{k},\mathbf{q}} \frac{f_{n\mathbf{k}} - f_{m\mathbf{k}+\mathbf{q}}}{\epsilon_{n\mathbf{k}} - \epsilon_{m\mathbf{k}+\mathbf{q}} + \omega} \times \overrightarrow{\psi}^{\dagger}_{n\mathbf{k}}(\mathbf{r})\, \sigma^i\, \overrightarrow{\psi}_{m\mathbf{k}+\mathbf{q}}(\mathbf{r})\, \overrightarrow{\psi}^{\dagger}_{m\mathbf{k}+\mathbf{q}}(\mathbf{r}')\, \sigma^j\, \overrightarrow{\psi}_{n\mathbf{k}}(\mathbf{r}'), \tag{15}$$

where $f_{n\mathbf{k}}$ and $f_{m\mathbf{k}+\mathbf{q}}$ are occupation numbers.

This formulation provides a two-step procedure for calculating the generalized susceptibility. First, the Kohn-Sham susceptibility is calculated via Eq. (15), starting from the unperturbed Kohn-Sham spinor wave functions. The computed $\chi^{ij}_{\rm KS}$ is then used inside Eq. (10) (after transforming to the frequency domain), so as as to evaluate χ^{ij} and obtain spin fluctuation spectra.

The main disadvantage of this procedure is that the evaluation of $\chi_{\rm KS}$ via Eq. (15) relies on the calculation of unoccupied Kohn-Sham states, and the convergence of the results with respect to the number of empty bands is slow. In order to circumvent this bottleneck, here we employ an alternative approach which is based on the Sternheimer equation [35] and which requires one to compute only occupied Kohn-Sham states.

B. Calculation of the spin susceptibility using the Sternheimer equation

The Sternheimer equation in time-dependent perturbation theory reads [17]:

$$\left(\hat{H} - i\frac{\partial}{\partial t}\hat{I}\right) \delta\overrightarrow{\psi}_{n\mathbf{k}}(\mathbf{r},t) = -(1 - \hat{P}_{\rm occ})\, \delta\hat{V}_{\rm scf}(\mathbf{r},t)\, \overrightarrow{\psi}_{n\mathbf{k}}(\mathbf{r}), \tag{16}$$

where $\hat{H}$ is the unperturbed Kohn-Sham Hamiltonian, corresponding to the term in square brackets in Eq. (1), $\delta\overrightarrow{\psi}_{n\mathbf{k}}$ is the first-order change of the spinor wave function, and $\delta\hat{V}_{\rm scf}$ is the first-order variation of the Kohn-Sham potential from Eq. (2). The operator $\hat{P}_{\rm occ}$ is the projector on the manifold of unoccupied Kohn-Sham states.

Equation (16) is naturally found as an intermediate step of the perturbation theory approach; by expressing $\delta\overrightarrow{\psi}_{n\mathbf{k}}$ in the frequency domain and expanding on a basis of (occupied and empty) Kohn-Sham states, this expression leads immediately to Eq. (15). In order to avoid the computation of unoccupied states, Eq. (16) must be solved directly as a nonhomogeneous linear system.

The Sternheimer equation was originally introduced for calculating the static dielectric polarizability of atoms [35] and found widespread use in the DFT community to compute phonon dispersion relations using DFPT [36–38]. The time-dependent version of the Sternheimer equation was used to calculate spin susceptibilities [17], dynamic molecular polarizabilities [39], and the screened Coulomb interaction in GW calculations [25–29,40].

We now consider an external perturbation given by a monochromatic plane wave:

$$\delta V^j_{\rm ext}(\mathbf{r}t) = \delta V^j_{\rm ext}(\mathbf{q},\omega)[e^{i(\mathbf{q}\cdot\mathbf{r}+\omega t)-\eta t} + \text{c.c.}], \tag{17}$$

with η being a positive infinitesimal. This perturbation induces a variation of the density matrix that can be evaluated using Eq. (16). After some lengthy but otherwise straightforward algebra one finds:

$$\delta\rho^i_{\mathbf{q}}(\mathbf{r},\omega) = \frac{1}{N_{\mathbf{k}}} \sum_{n\in{\rm occ},\mathbf{k}} \overrightarrow{u}^{\dagger}_{n\mathbf{k}}(\mathbf{r})\, \sigma^i\, \delta\overrightarrow{u}_{n\mathbf{k}+\mathbf{q}}(\mathbf{r},\omega) + \frac{1}{N_{\mathbf{k}}} \sum_{n\in{\rm occ},\mathbf{k}} \delta\overrightarrow{u}^{\dagger}_{n\mathbf{k}-\mathbf{q}}(\mathbf{r},-\omega)\, \sigma^i\, \overrightarrow{u}_{n\mathbf{k}}(\mathbf{r}), \tag{18}$$

where $\overrightarrow{u}_{n\mathbf{k}}$ is the Bloch-periodic part of the Kohn-Sham wave function, i.e., $\overrightarrow{\psi}_{n\mathbf{k}}(\mathbf{r}) = e^{i\mathbf{k}\cdot\mathbf{r}}\overrightarrow{u}_{n\mathbf{k}}(\mathbf{r})$, and similarly for $\delta\overrightarrow{u}_{n\mathbf{k}+\mathbf{q}}(\mathbf{r},\omega)$ and $\delta\rho^i_{\mathbf{q}}(\mathbf{r},\omega)$. The variation of the Kohn-Sham wave functions appearing in the last expression can be found from Eq. (16), following the usual decoupling procedure employed in DFPT for phonons [36]:

$$(\hat{H}_{\mathbf{k}+\mathbf{q}} - \epsilon_{n\mathbf{k}} + \omega + i\eta)\, \delta\overrightarrow{u}_{n\mathbf{k}+\mathbf{q}}(\mathbf{r},+\omega) = -\left(1 - \hat{P}^{\mathbf{k}+\mathbf{q}}_{\rm occ}\right) \delta\hat{V}^{+\mathbf{q}}_{\rm scf}(\mathbf{r},+\omega)\, \overrightarrow{u}_{n\mathbf{k}}(\mathbf{r}), \tag{19}$$

$$(\hat{H}_{\mathbf{k}-\mathbf{q}} - \epsilon_{n\mathbf{k}} - \omega + i\eta)\, \delta\overrightarrow{u}_{n\mathbf{k}-\mathbf{q}}(\mathbf{r},-\omega) = -\left(1 - \hat{P}^{\mathbf{k}-\mathbf{q}}_{\rm occ}\right) \delta\hat{V}^{-\mathbf{q}}_{\rm scf}(\mathbf{r},-\omega)\, \overrightarrow{u}_{n\mathbf{k}}(\mathbf{r}). \tag{20}$$

Here $\hat{H}_{\mathbf{k}}$ denotes the $\mathbf{k}$-projected unperturbed Kohn-Sham Hamiltonian. Similarly $\hat{P}^{\mathbf{k}}_{\rm occ}$ indicates the component of the projector operator on the occupied states with wave-vector $\mathbf{k}$. $\delta\hat{V}^{+\mathbf{q}}_{\rm scf}(\mathbf{r},\omega)$ is the Bloch-periodic component of the self-consistent variation of the Kohn-Sham potential, for the wave vector $+\mathbf{q}$.

The variation of the self-consistent potential is related to the variation of the charge density as follows:

$$\delta\hat{V}^{\mathbf{q}}_{\rm scf}(\mathbf{r},\omega) = \sigma^j\, \delta V^j_{\rm ext}(\mathbf{q},\omega) + \sigma^0 \int \frac{\delta\rho^0_{\mathbf{q}}(\mathbf{r}',\omega)}{|\mathbf{r}-\mathbf{r}'|} e^{-i\mathbf{q}\cdot(\mathbf{r}-\mathbf{r}')} d\mathbf{r}' + \sum_{ij} \sigma^i\, f^{ij}_{xc}[\rho(\mathbf{r}),\mathbf{r}]\, \delta\rho^j_{\mathbf{q}}(\mathbf{r},\omega), \tag{21}$$

where the integration in the second line is in the unit cell, and the exchange-correlation kernel in the third line is evaluated for the unperturbed density. From Eq. (20) we see that, in addition

to $\delta\hat{V}^{\mathbf{q}}_{\mathrm{scf}}(\mathbf{r},\omega)$, we also need $\delta\hat{V}^{-\mathbf{q}}_{\mathrm{scf}}(\mathbf{r},-\omega)$. In order to evaluate this term via Eq. (21) we simply change the signs of $\mathbf{q}$ and ω and observe that $\delta\rho^{i}_{-\mathbf{q}}(\mathbf{r},-\omega)=\delta\rho^{i*}_{\mathbf{q}}(\mathbf{r},\omega)$.

Equations (18)–(21) are to be solved self-consistently. The procedure starts from Eq. (21), by setting the initial variation of the Kohn-Sham potential equal to the external perturbation (i.e., by retaining only the first line). Then Eqs. (19) and (20) are solved, and the solutions are used in Eq. (18) to obtain $\delta\rho^{i}_{\mathbf{q}}(\mathbf{r},\omega)$. We emphasize that the presence of an external magnetic field breaks time reversal symmetry, therefore Eqs. (19) and (20) have to be solved *separately*. This is in contrast to what happens in DFPT for phonons, whereby these two equations become equivalent after taking into account time-reversal symmetry [36].

The self-consistent solution of Eqs. (18)–(21) yields the variation $\delta\rho^{j}_{\mathbf{q}}(\mathbf{r},\omega)$ of the density matrix in response to the external perturbation of Eq. (17). By taking the unit-cell average of the density variation, $\delta\rho^{i}(\mathbf{q},\omega)=\int d\mathbf{r}\,\delta\rho^{j}_{\mathbf{q}}(\mathbf{r},\omega)$, we can finally calculate the susceptibility as:

$$\chi^{ij}(\mathbf{q},\omega)=\frac{\delta\rho^{i}(\mathbf{q},\omega)}{\delta V^{j}_{\mathrm{ext}}(\mathbf{q},\omega)}. \tag{22}$$

Furthermore, this quantity can directly be compared with experiments. For example, in a ferromagnet with the spin density polarized along the z direction, the transverse component of spin susceptibility, defined as $\chi^{+-}=\chi^{11}-i\chi^{12}$, yields the inelastic neutron scattering cross section according to the equation [41]:

$$\frac{\partial^2\Sigma}{\partial\Omega\partial\omega}\propto \mathrm{Im}\,\chi^{+-}(\mathbf{q},\omega), \tag{23}$$

where $\mathbf{q}$ and ω have the meaning of momentum and energy transfer, respectively, and $\partial\Omega$ is the element of solid angle spanned by $\mathbf{q}$. Sharp peaks of $\mathrm{Im}\chi^{+-}$ in the $(\mathbf{q},\omega)$ plane correspond to magnon excitations [1].

Magnon excitation are expected to be damped in the presence of resonant Stoner spin-flip excitations. The region in the $(\mathbf{q},\omega)$ plane where Stoner excitations are allowed corresponds to energy and momenta for which the noninteracting susceptibility, $\mathrm{Im}\,\chi^{+-}_{\mathrm{KS}}(\mathbf{q},\omega)$, is nonzero [1]. In fact, by performing a Fourier transform of Eq. (15), we find immediately:

$$\mathrm{Im}\,\chi^{+-}_{\mathrm{KS}}(\mathbf{q},\omega)=\frac{\pi}{2}\frac{1}{N_{\mathbf{k}}}\sum_{nm,\mathbf{k}}(f_{n\mathbf{k}}-f_{m\mathbf{k}+\mathbf{q}}) \times|\langle\overrightarrow{u}_{m\mathbf{k}+\mathbf{q}}|\sigma^{-}|\overrightarrow{u}_{n\mathbf{k}}\rangle|^2\delta(\epsilon_{n\mathbf{k}}-\epsilon_{m\mathbf{k}+\mathbf{q}}+\omega), \tag{24}$$

where $\sigma^{-}=\sigma^{1}-i\sigma^{2}$. The r.h.s. of this expression corresponds to the standard transition rate as given by the Fermi golden rule, with respect to an operator which lowers the spin quantum number in a ferromagnet. We note that our approach avoids storage of the whole susceptibility matrix, which requires a memory of size proportional to the square of the number of plane waves.

C. Fractional occupations

The formalism described in the previous section is applicable to insulators and semiconductors, where the occupied and unoccupied states are separated by a finite energy gap. In principle, the formalism also applies for metals at zero temperature. However, in the case of metals, a very dense sampling of the Brillouin zone would be required to correctly describe the Fermi surface. To avoid this complication in the case of metals, it is common to perform Brillouin zone integrals using the tetrahedron method [37,42,43] or to employ smearing techniques [36,44]. In this work we opted for the use of electronic smearing, and in the following we discuss how the formalism introduced in Ref. [44] needs to be adapted to deal with frequency-dependent perturbations and spinor wave functions.

In the scheme of Ref. [44] each Kohn-Sham energy level is broadened by a smearing function defined by $\delta_\gamma(\epsilon)=\tilde{\delta}(\epsilon/\gamma)/\gamma$. Here $\tilde{\delta}(x)$ is a normalized function such that $\delta_\gamma(x)$ tends to the Dirac δ function when the smearing width γ tends to zero. The simplest smearing function is a Gaussian but there are many practical alternatives [30]. From the definition of δ_γ one naturally obtains a smooth approximation to the step function, $\theta(\tilde{x})=\int_{-\infty}^{x}\tilde{\delta}(x')dx'$. The convergence of our results with respect to γ is discussed in Appendix A.

Following Ref. [44] we define $\tilde{\theta}_{n,m}=\tilde{\theta}[(\epsilon_n-\epsilon_m)/\gamma]$, and $\tilde{\theta}_{\mathrm{F},m}=\tilde{\theta}[(\epsilon_{\mathrm{F}}-\epsilon_m)/\gamma]$, with ϵ_{F} the Fermi energy. Using these definitions the smeared density matrix reads:

$$\rho^{i}(\mathbf{r})=\frac{1}{N_{\mathbf{k}}}\sum_{n\mathbf{k}}\tilde{\theta}_{\mathrm{F},n\mathbf{k}}\,\overrightarrow{u}^{\dagger}_{n\mathbf{k}}(\mathbf{r})\,\sigma^{i}\,\overrightarrow{u}_{n\mathbf{k}}(\mathbf{r}), \tag{25}$$

where the sum is over all states n. Since $\tilde{\theta}$ is a smeared step function, it is sufficient to only calculate all occupied states and a handful of unoccupied states, up to the energy $\sim\epsilon_{\mathrm{F}}+10\gamma$. The linear density response to an external monochromatic perturbation as in Eq. (17) reads:

$$\delta\rho^{i}_{\mathbf{q}}(\mathbf{r},\omega)=\frac{1}{N_{\mathbf{k}}}\sum_{n\mathbf{k}}\tilde{\theta}_{F,n\mathbf{k}}\,\overrightarrow{u}^{\dagger}_{n\mathbf{k}}(\mathbf{r})\,\sigma^{i}\,\delta\overrightarrow{u}_{n\mathbf{k}+\mathbf{q}}(\mathbf{r},\omega) + \frac{1}{N_{\mathbf{k}}}\sum_{n\mathbf{k}}\tilde{\theta}_{F,n\mathbf{k}}\,\delta\overrightarrow{u}^{\dagger}_{n\mathbf{k}-\mathbf{q}}(\mathbf{r},-\omega)\,\sigma^{i}\,\overrightarrow{u}_{n\mathbf{k}}(\mathbf{r}). \tag{26}$$

In this expression we are neglecting the contribution to the density variation arising from a change in the Fermi level, which corresponds formally to the variation of the prefactor $\tilde{\theta}_{F,n\mathbf{k}}$. This contribution is only important for $\mathbf{q}=0$, and it vanishes for the perturbations considered in this paper.

The linear variation of the spinor wave function can be formally written using perturbation theory:

$$\delta\overrightarrow{u}_{n\mathbf{k}+\mathbf{q}}(\mathbf{r},\omega)=\sum_{m}\frac{\overrightarrow{u}_{m\mathbf{k}+\mathbf{q}}\langle\overrightarrow{u}_{m\mathbf{k}+\mathbf{q}}|\delta\hat{V}^{\mathbf{q}}_{\mathrm{scf}}(\mathbf{r},\omega)|\overrightarrow{u}_{n\mathbf{k}}\rangle}{\epsilon_{n\mathbf{k}}-\epsilon_{m\mathbf{k}+\mathbf{q}}+\omega-i\eta}, \tag{27}$$

and similarly for $\delta\overrightarrow{u}_{n\mathbf{k}-\mathbf{q}}(\mathbf{r},-\omega)$. After replacing this expression in Eq. (26) one obtains:

$$\delta\rho^{i}_{\mathbf{q}}(\mathbf{r},\omega)=\frac{1}{N_{\mathbf{k}}}\sum_{nm,\mathbf{k}}(\tilde{\theta}_{F,n\mathbf{k}}-\tilde{\theta}_{F,m\mathbf{k}+\mathbf{q}}) \times\frac{\overrightarrow{u}^{\dagger}_{n\mathbf{k}}\sigma^{i}\overrightarrow{u}_{m\mathbf{k}+\mathbf{q}}\langle\overrightarrow{u}_{m\mathbf{k}+\mathbf{q}}|\delta\hat{V}^{\mathbf{q}}_{\mathrm{scf}}(\mathbf{r},\omega)|\overrightarrow{u}_{n\mathbf{k}}\rangle}{\epsilon_{n\mathbf{k}}-\epsilon_{m\mathbf{k}+\mathbf{q}}+\omega-i\eta}. \tag{28}$$

To obtain a more compact expression, in the second line of Eq. (26) we replaced $\mathbf{k}$ by $\mathbf{k}+\mathbf{q}$ and m by n, and we used the identity $\delta\hat{V}^{-\mathbf{q}}_{\rm scf}(\mathbf{r},-\omega)^\dagger = \delta\hat{V}^{\mathbf{q}}_{\rm scf}(\mathbf{r},\omega)$.

Equation (28) contains a summation over all states, occupied and empty. In order to recast this expression into a sum over occupied states only, we observe that the prefactor $\tilde{\theta}_{F,n\mathbf{k}} - \tilde{\theta}_{F,m\mathbf{k}+\mathbf{q}}$ vanishes when the states $n\mathbf{k}$ and $m\mathbf{k}+\mathbf{q}$ are both occupied or both unoccupied. This observation can be used to bring Eq. (28) into a form similar to Eq. (26), but without the $\tilde{\theta}$ prefactors. To this aim we note that $\tilde{\theta}(x)+\tilde{\theta}(-x)=1$, therefore Eq. (28) can be rewritten as:

$$\delta\rho^i_{\mathbf{q}}(\mathbf{r},\omega) = \frac{1}{N_{\mathbf{k}}}\sum_{nm,\mathbf{k}} (\tilde{\theta}_{F,n\mathbf{k}} - \tilde{\theta}_{F,m\mathbf{k}+\mathbf{q}})\tilde{\theta}_{m\mathbf{k}+\mathbf{q},n\mathbf{k}} \frac{\overrightarrow{u}^\dagger_{n\mathbf{k}}\sigma^i\overrightarrow{u}_{m\mathbf{k}+\mathbf{q}}\langle\overrightarrow{u}_{m\mathbf{k}+\mathbf{q}}|\delta\hat{V}^{\mathbf{q}}_{\rm scf}(\mathbf{r},\ \omega)|\overrightarrow{u}_{n\mathbf{k}}\rangle}{\epsilon_{n\mathbf{k}} - \epsilon_{m\mathbf{k}+\mathbf{q}} + \omega - i\eta}$$
$$+ \frac{1}{N_{\mathbf{k}}}\sum_{nm,\mathbf{k}}\left[(\tilde{\theta}_{F,n\mathbf{k}} - \tilde{\theta}_{F,m\mathbf{k}-\mathbf{q}})\tilde{\theta}_{m\mathbf{k}-\mathbf{q},n\mathbf{k}} \frac{\overrightarrow{u}^\dagger_{n\mathbf{k}}\sigma^i\overrightarrow{u}_{m\mathbf{k}-\mathbf{q}}\langle\overrightarrow{u}_{m\mathbf{k}-\mathbf{q}}|\delta\hat{V}^{-\mathbf{q}}_{\rm scf}(\mathbf{r},-\omega)|\overrightarrow{u}_{n\mathbf{k}}\rangle}{\epsilon_{n\mathbf{k}} - \epsilon_{m\mathbf{k}-\mathbf{q}} - \omega - i\eta}\right]^\dagger. \quad (29)$$

Also in this case the second line has been rewritten by exchanging $\mathbf{k}$ and $\mathbf{k}-\mathbf{q}$, n and m, and using $\delta\hat{V}^{-\mathbf{q}}_{\rm scf}(\mathbf{r},-\omega)^\dagger = \delta\hat{V}^{\mathbf{q}}_{\rm scf}(\mathbf{r},\omega)$. By inspecting the terms $(\tilde{\theta}_{F,n\mathbf{k}} - \tilde{\theta}_{F,m\mathbf{k}+\mathbf{q}})\tilde{\theta}_{m\mathbf{k}+\mathbf{q},n\mathbf{k}}$ we can see that now the summation over n effectively runs over occupied states, and that over m runs over unoccupied states. At this point it is a matter of algebra to show that the density matrix variation can be written compactly as follows:

$$\delta\rho^i_{\mathbf{q}}(\mathbf{r},\omega) = \frac{1}{N_{\mathbf{k}}}\sum_{n\mathbf{k}} \overrightarrow{u}^\dagger_{n\mathbf{k}}(\mathbf{r})\,\sigma^i\,\delta\overrightarrow{v}_{n\mathbf{k}+\mathbf{q}}(\mathbf{r},\omega)$$
$$+ \frac{1}{N_{\mathbf{k}}}\sum_{n\mathbf{k}} \delta\overrightarrow{v}^\dagger_{n\mathbf{k}-\mathbf{q}}(\mathbf{r},-\omega)\,\sigma^i\,\overrightarrow{u}_{n\mathbf{k}}(\mathbf{r}), \quad (30)$$

where $\delta\overrightarrow{v}_{n\mathbf{k}+\mathbf{q}}(\mathbf{r},\omega)$ is the solution of the *modified* Sternheimer equation:

$$(\hat{H}_{\mathbf{k}+\mathbf{q}} + \alpha\hat{Q}_{\mathbf{k}+\mathbf{q}} - \epsilon_{n\mathbf{k}} - \omega + i\eta)\,\delta\overrightarrow{v}_{n\mathbf{k}+\mathbf{q}}(\mathbf{r},+\omega)$$
$$= -(\tilde{\theta}_{F,n\mathbf{k}} - \hat{P}^{+\omega}_{n,\mathbf{k}+\mathbf{q}})\,\delta\hat{V}^{+\mathbf{q}}_{\rm scf}(\mathbf{r},+\omega)\overrightarrow{u}_{n\mathbf{k}}(\mathbf{r}). \quad (31)$$

In this equation α is a real parameter to be discussed below, and the projector operators are defined as:

$$\hat{Q}_{\mathbf{k}+\mathbf{q}} = \sum\nolimits_m |\overrightarrow{u}_{m\mathbf{k}+\mathbf{q}}\rangle\langle\overrightarrow{u}_{m\mathbf{k}+\mathbf{q}}|, \quad (32)$$

$$\hat{P}^{+\omega}_{n,\mathbf{k}+\mathbf{q}} = \sum\nolimits_m \beta^{+\omega}_{nm,\mathbf{k}+\mathbf{q}}|\overrightarrow{u}_{m\mathbf{k}+\mathbf{q}}\rangle\langle\overrightarrow{u}_{m\mathbf{k}+\mathbf{q}}|, \quad (33)$$

with the summation running over the occupied states plus a few empty states, as discussed for Eq. (25). The parameters $\beta^{+}_{nm,\mathbf{k}+\mathbf{q}}$ are given by:

$$\beta^{+\omega}_{nm,\mathbf{k}+\mathbf{q}} = \tilde{\theta}_{F,n\mathbf{k}}\,\tilde{\theta}_{n\mathbf{k},m\mathbf{k}+\mathbf{q}} + \tilde{\theta}_{F,m\mathbf{k}+\mathbf{q}}\,\tilde{\theta}_{m\mathbf{k}+\mathbf{q},n\mathbf{k}}$$
$$+ \alpha\frac{(\tilde{\theta}_{F,n\mathbf{k}} - \tilde{\theta}_{F,m\mathbf{k}+\mathbf{q}})\tilde{\theta}_{m\mathbf{k}+\mathbf{q},n\mathbf{k}}}{\epsilon_{n\mathbf{k}} - \epsilon_{m\mathbf{k}+\mathbf{q}} + \omega - i\eta}. \quad (34)$$

An equation analogous to Eq. (31) is obtained for the function $\delta\overrightarrow{v}_{n\mathbf{k}-\mathbf{q}}(\mathbf{r},-\omega)$ needed in Eq. (30). In practice one only needs to change the signs of $\mathbf{q}$ and ω in Eqs. (31)–(34). In order to derive Eqs. (30)–(34) starting from Eq. (29) it is sufficient to act on the first line of the r.h.s. with the operator $\epsilon_{n\mathbf{k}} - (\hat{H}_{\mathbf{k}+\mathbf{q}} + \alpha\hat{Q}_{\mathbf{k}+\mathbf{q}}) + \omega - i\eta$. These equations constitute a straightforward generalization of the treatment of fractional occupations in standard DFPT for phonons [36,44].

As in the case of phonon calculations, the parameter α appearing in Eq. (31) is chosen so as to make the linear operator on the l.h.s. nonsingular. When choosing $\eta=0$, the system can become singular if $\epsilon_{m\mathbf{k}+\mathbf{q}}$ is in resonance with $\epsilon_{n\mathbf{k}}+\omega$, where n belongs to the manifold of occupied states. To avoid a singularity it therefore suffices to choose $\alpha = \epsilon_F - \epsilon_{\rm min} + \omega_{\rm max} + 10\gamma$, where $\epsilon_{\rm min}$ is the smallest eigenvalue of the occupied manifold, and $\omega_{\rm max}$ is the highest frequency considered in the calculations. If we set instead $\eta>0$, the calculation is effectively performed for a complex frequency, and strictly speaking the linear system cannot become singular. However, the use of the projector $\alpha\hat{Q}_{\mathbf{k}+\mathbf{q}}$ is still important in order to reduce the condition number of the linear system.

D. Symmetry reduction

The summation over $\mathbf{k}$ points in the Brillouin zone in Eq. (30) can effectively be performed by exploiting crystal symmetry operations. In standard DFPT symmetry is used to reduce the set of $\mathbf{k}$ points to a symmetry-irreducible wedge of the Brillouin zone [30].

In the present work we are dealing with DFPT in the presence of spinor wave functions, therefore we also need to take into account the effect of symmetry operations on the electron spins. To this aim we make use of spin-space groups (SSG) [45]. The action of an element $\mathcal{S}$ of the SSG on a spinor wave funtion can be described as:

$$\mathcal{S}:\{R_s|R|f\}\overrightarrow{\psi}(\mathbf{r}) = R_s\overrightarrow{\psi}(R^{-1}\mathbf{r}-\mathbf{f}), \quad (35)$$

where R is the spacial rotation, $\mathbf{f}$ is the possible fractional translation, and R_s is the matrix that rotates the spins.

Generally speaking one could also consider time-reversal symmetry in order to perform further reductions of the number of required $\mathbf{k}$ points. Time reversal can be combined with operations in the SSG [45]. However, since in our present work we are focusing on perturbations corresponding to magnetic fields, time-reversal symmetry is broken. As a result we can only consider symmetry operations in the SSG which do not involve time reversal. In practice we perform symmetry reduction by considering all the symmetry operations $\mathcal{S}$ which do not contain time reversal and which belong to the small group of $\mathbf{q}$, where $\mathbf{q}$ is the wave vector of the perturbation (the small group is the subgroup of elements which leave $\mathbf{q}$ unchanged, $\mathcal{S}\mathbf{q}=\mathbf{q}$).

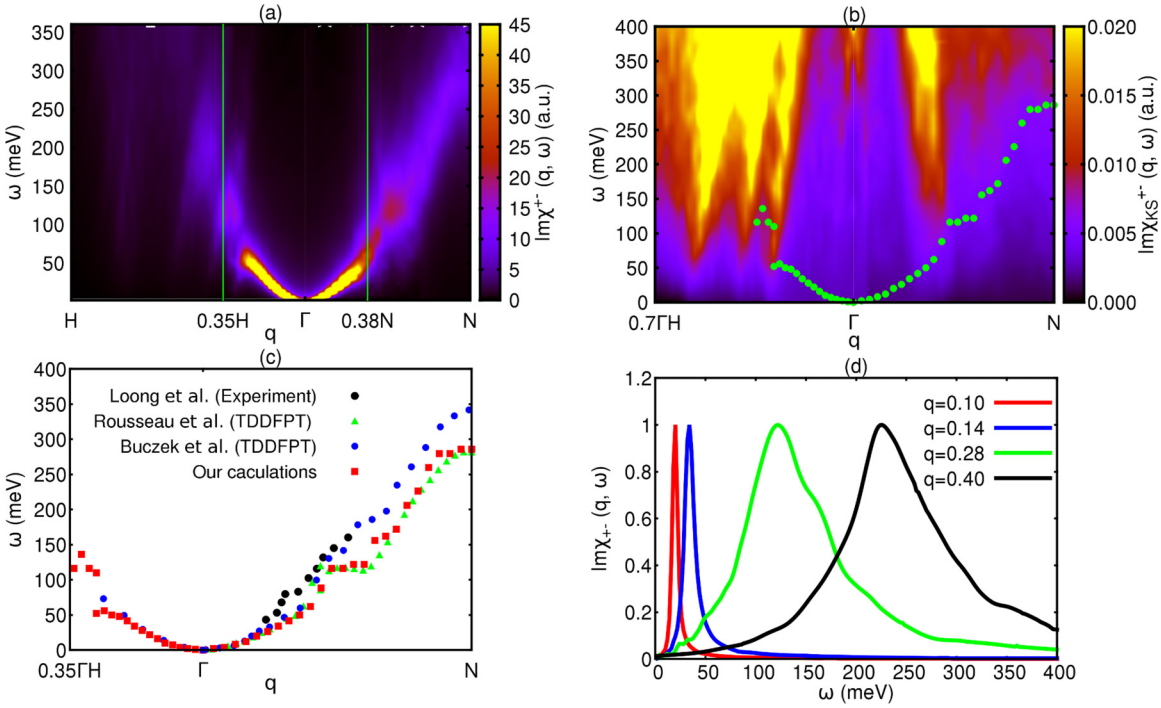

FIG. 1. (a) Calculated $\mathrm{Im}\chi^{+-}(\mathbf{q},\omega)$ of Fe along the ΓN and ΓH directions. The susceptibility is given in atomic units, $1/(\mathrm{Ry\,bohr}^3)$. (b) Calculated $\mathrm{Im}\chi^{+-}_{\mathrm{KS}}(\mathbf{q},\omega)$ along the ΓN and ΓH directions. We also show the magnon dispersion curves superimposed as dots. (c) Magnon bands of Fe along the ΓN and ΓH directions. We compare our results to the experimental data of Loong *et al.* [55], and the calculations of Rousseau *et al.* [18], and Buczek *et al.* [15]. (d) Calculated $\mathrm{Im}\chi^{+-}(\mathbf{q},\omega)$ of Fe, for selected wave vectors along the ΓN direction. All peaks are normalized to their maximum for clarity, and the wave vectors are given as $\mathbf{q} = 2\pi/a(1,1,0)q$.

E. Implementation details

The method described in the preceding sections was implemented using plane-waves basis sets and pseudopotentials, starting from the linear response modules of the QUANTUM ESPRESSO suite, and in particular from the PHONON code [30]. The development version of this code is hosted on our GitHub repository [31]. We have support for both norm-conserving [46] and ultrasoft [47] pseudopotentials. Since we only consider the coupling between magnetic field and the spin degree of freedom, our implementation is expected not to suffer from gauge invariance issues, which are known to be present when orbital magnetism is taken into account in magnetic response calculations [48,49].

In our implementation the Sternheimer equation, Eq. (30), is solved separately for each frequency ω using the complex biconjugate gradient method, as described in Ref. [50]. The implementation was adapted from related work within the context of GW calculations from Refs. [25,29].

In order to minimize fluctuations of the density matrix during the self-consistent iterations, we employed a generalization of the modified Broyden method for charge-density mixing [51], following Ref. [25]. We found that typically five iterations are enough to reach convergence in the self-consistent calculation.

In this method we need to solve Eq. (30) both for the $(+\mathbf{q}, +\omega)$ channel and the $(-\mathbf{q}, -\omega)$ channel. The solutions for each channel are evaluated separately and independently. The parallelization of the algorithm is on the **k** points within each channel. In all the calculations reported below we employed a parameter $\alpha = 500$ meV in Eq. (30), which lies above the highest magnon energy calculated in the three examples.

III. RESULTS

In order to test our implementation we performed calculations on three representative elemental transition metals, namely bcc iron, fcc nickel, and bcc chromium. Ground-state DFT calculations were performed using QUANTUM ESPRESSO, within the local density approximation for the exchange and correlation [52], and using pseudopotentials from the repository 'PSlibrary 0.3.1' [53].

When performing calculations of spin fluctuations, the ground state calculation and the solution of the Sternheimer equation must be carried out using the *same* sampling of the Brillouin zone. This is necessary in order to avoid spurious symmetry breaking leading to the so-called gap error, that is the presence of long-wavelength magnons with finite excitation energy [15,18,54]. This aspect is discussed in more details in Appendix B. In all the following calculations we employed a $50 \times 50 \times 50$ grid of **k** points for calculating both the ground state and the spin fluctuation spectra.

Below, when comparing with previous work, we only include the most recent theoretical studies. A more detailed comparison between earlier theoretical results can be found in Refs. [18,32].

A. BCC iron

We performed calculations using a norm conserving pseudopotential [46], using a plane-waves kinetic energy cutoff of

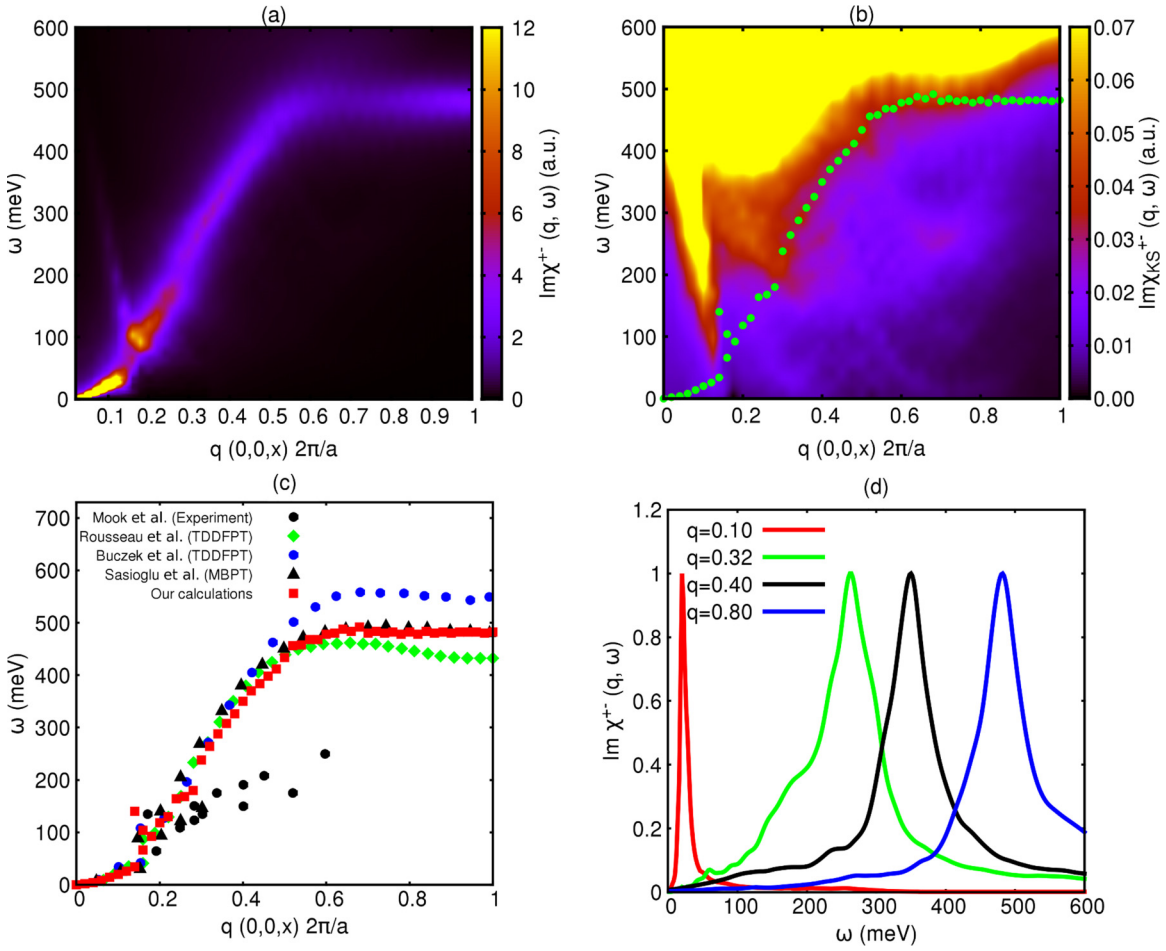

FIG. 2. (a) Calculated $\mathrm{Im}\,\chi^{+-}(\mathbf{q},\omega)$ of Ni along the ΓX direction. (b) Calculated $\mathrm{Im}\,\chi^{+-}_{\mathrm{KS}}(\mathbf{q},\omega)$, with the magnon band superimposed as dots. (c) Calculated magnon dispersion curve of Ni along the ΓX direction. Our results are compared with experimental data of Mook *et al.* [56,57], and with the calculations of Rousseau *et al.* [18], Buczek *et al.* [15], using TD-DFPT, and Şaşıoğlu *et al.* [33] using many body perturbation theory (MBPT). (d) Calculated $\mathrm{Im}\,\chi^{+-}(\mathbf{q},\omega)$ of Ni for selected wave vectors along the ΓX direction. The peaks are normalized to their maximum value, and the wave vector is given as $\mathbf{q} = 2\pi/a(1,0,0)q$.

60 Ry. To deal with fractional occupations we used a Gaussian smearing with a width of 10 mRy. We employed the experimental lattice parameter $a = 5.406$ bohr. Our calculations yield a ground-state magnetization of $2.16\,\mu_{\mathrm{B}}$ per atom, and the mean Stoner splitting is 2.5 eV. We evaluated the transverse spin susceptibility $\chi^{+-}(\mathbf{q},\omega)$ for wave vectors $\mathbf{q}$ along the ΓN and the ΓH high-symmetry lines [N $= (1/2,1/2,0)2\pi/a$, H $= (0,0,1)2\pi/a$]. We sampled the frequency axis in the range 0 to 400 meV, with a spacing of 2 meV between consecutive grid points. The broadening parameter was set to $\eta = 0.1\,\omega$; this choice was motivated by the observation that a larger broadening is required to obtain converged spectra at higher frequencies.

The calculations are shown in Fig. 1. In particular, Fig. 1(a) shows a two-dimensional plot of $\mathrm{Im}\,\chi^{+-}$ in the $(\mathbf{q},\omega)$ plane. For clarity we also report some cuts for a few selected wave vectors in Fig. 1(d). The maxima of the map in Fig. 1(a) are reported in the form of magnon frequency-wave-vector dispersion relations in Fig. 1(c). The map of Fig. 1(a) shows a significant attenuation of the magnon resonances beyond $|\mathbf{q}| \sim 0.38$ ΓN, nevertheless we can clearly recognize the magnon excitations all the way up to the Brillouin zone edge. Along the ΓH line instead, magnon excitations are so strongly damped beyond $|\mathbf{q}| \sim 0.35$ ΓH that no clear curve can be identified in this region. The difference in the magnon damping patterns along the two directions is a direct consequence of the anisotropic nature of the Stoner continuum, as is seen in Fig. 1(b). Here we see that along ΓH Stoner excitations become possible already around 100 meV, causing the complete suppression of magnons with energies above this threshold.

In Fig. 1(c) we also compare our results with previous experimental and theoretical work. Along the ΓN direction our magnon dispersion curve is in excellent agreement with the results of Ref. [18]. This level of agreement was to be expected since also the implementation of Ref. [18] is based on the QUANTUM ESPRESSO package, although these authors used the method described in Sec. II A instead of the Sternheimer equation. As pointed out in Ref. [18], theoretical results tend to differ significantly beyond $|\mathbf{q}| \sim 0.4$ΓN.

We note that a double-peak structure is observed in the calculated spectra at $|\mathbf{q}| = 0.5$ΓN in Ref. [32] and at $|\mathbf{q}| = 0.4375$ΓN in Ref. [18], yielding a gap in the corresponding magnon dispersion. In agreement with Refs. [15,17], here we do not observe double-peak structures. However, our magnon

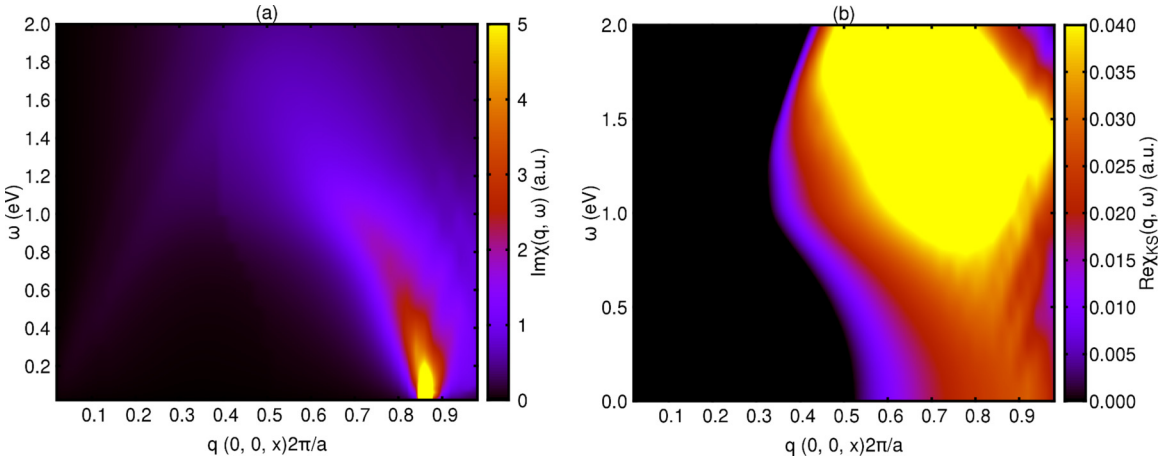

FIG. 3. (a) Calculated $\mathrm{Im}\chi(\mathbf{q},\omega)$ of Cr along the ΓH direction. (b) Calculated $\mathrm{Re}\chi_{\mathrm{KS}}(\mathbf{q},\omega)$ of Cr along the ΓH direction. To highlight the effect of Fermi-surface nesting, we plot $\mathrm{Re}\chi_{\mathrm{KS}}(\mathbf{q},\omega) - 0.2$ and only show the positive values.

spectra around $|\mathbf{q}| = 0.5\Gamma\mathrm{N}$ is significantly broadened, and this is consistent with the fact that the double-peak structure in Ref. [32] is not as prominent as that found in typical two-branch magnon spectra. More notably, our calculations yield a plateau around $|\mathbf{q}| \sim 0.5\Gamma\mathrm{N}$, while Refs. [15,17] report a monotonic curve. We also observe that the discrepancies lie in the region where Stoner excitations kick in. It is likely that these differences between the various approaches arise from the difference in the underlying ground-state DFT calculations. Along the ΓH direction our results are in agreement with those of Ref. [15], which also find a strong suppression of spin waves in the same range of wave vectors. Our calculations are in reasonable agreement with the low-temperature experimental data of Ref. [55] (taken at 10 K). One aspect which complicates the comparison between theory and experiment is that the measurements were not taken exactly along the ΓN or ΓH lines. Having more information on the precise wave-vector path probed in the experiments would be useful to perform a more detailed comparison.

B. FCC nickel

In this case we performed calculations using an ultrasoft pseudopotential [47], using a plane-waves kinetic energy cutoff of 42 Ry for the wave function and a cutoff of 236 Ry for the charge density. We employed Marzari-Vanderbilt smearing [58] with a broadening parameter of 10 mRy. We used the experimental lattice parameter $a = 6.65$ bohr. We obtained a ground-state magnetization of 0.61 μ_{B} per atom and the mean Stoner splitting of 0.66 eV. We computed $\chi^{+-}(\mathbf{q},\omega)$ along the ΓX direction [$\mathrm{X} = (0,0,1)2\pi/a$]. We sampled frequencies up to 600 meV with a grid spacing of 2 meV and a broadening parameter $\eta = 0.1\,\omega$.

The calculated susceptibility is shown as a two-dimensional $(\mathbf{q},\omega)$ map in Fig. 2(a). Also in this case we show representative cuts at selected wave vectors in Fig. 2(d). From the map we recognize a well-defined magnon band along the ΓX line. The excitation spectrum is sharp up to $|\mathbf{q}| \sim 0.3\Gamma\mathrm{X}$ and becomes broadened upon entering the Stoner continuum beyond this point. This effect is clearly seen in Fig. 2(b), where we superimpose the spin wave dispersion curve to the Stoner spectrum. Our calculated magnon band, as extracted from the maxima of $\mathrm{Im}\chi^{+-}(\mathbf{q},\omega)$, is compared to previous calculations and experiments in Fig. 2(c). Here we observe that theoretical data agree well for small wave vectors, but start deviating significantly from each other near the zone boundary, which is also observed in Ref. [18]. We tentatively assign these deviations to the different choices employed to describe the ground-state electronic structure.

In Fig. 2(a), two magnon branches are observed in a narrow area around $|\mathbf{q}| = 0.15\Gamma\mathrm{X}$. Similar observations were reported in Refs. [15,18] as well as in Refs. [17,32,33] where the two branches exist in a wider area. This is consistent with experimental observations where so called optical magnons are detected [56,57]. The optical magnons are a manifestation of itinerant magnetism effect since in the localized moment picture there is only one spin degree of freedom in monoatomic Ni. However, the two branches show similar magnetization profiles, in contrast to optical magnons in diatomic systems, such as hexagonal Co [15].

In further comparison with experiment we see that our calculations, as well as previous theoretical data, consistently overestimate the experiments by up to a factor of two. This phenomenon is well understood and is related to the fact that the Stoner splitting of fcc Ni in standard DFT is approximately twice as large as in experiment (0.66 eV vs 0.3 eV, respectively) [33,59,60]. It was shown that the experimental magnon spectra can be reasonably reproduced by manually reducing the LSDA exchange splitting by one half [32,33].

C. BCC chromium

For chromium we used a norm-conserving pseudopotential with a cutoff of 60 Ry and a Gaussian smearing of 10 mRy. We set the lattice parameter to the experimental value $a = 5.5$ bohr. We evaluated the susceptibility along the ΓH line, and we sampled frequencies using a grid spacing of 20 meV, up to a maximum value of 2 eV. In this case we used a constant broadening parameter $\eta = 100$ meV.

Experiments indicate that the ground-state electronic structure of Cr is a spin-density wave (SDW), with an incommensurate wave vector $\mathbf{q}_{\mathrm{SDW}} \simeq (0,0,0.95)2\pi/a$ [61]. This SDW

was attributed to the presence of pronounced Fermi-surface nesting in paramagnetic Cr [62–64], a scenario which was later confirmed by explicit DFT calculations [65].

The calculated spin susceptibility of paramagnetic Cr is shown in Fig. 3(a). Here we see a clear peak for wave vectors around $(0,0,0.86)2\pi/a$, extending down to zero excitation energy. The presence of zero-energy excitations at finite wave vector is the signature of a SDW, i.e., a frozen spin wave, analogous to charge-density waves observed in the presence of soft phonons. The role of Fermi-surface nesting can be investigated by inspecting the nesting function, that is $\mathrm{Re}\,\chi_{\mathrm{KS}}(\mathbf{q},\omega)$, as shown in Fig. 3(b). For $\omega = 0$ the nesting function reaches a maximum at $\mathbf{q}_{\mathrm{nest}} \sim (0,0,0.92)2\pi/a$, which is close to our calculated SDW vector. This result confirms that nesting is at the origin of the SDW in chromium.

Our present results are in good agreement with previous calculations [17], although we obtain a slightly shorter SDW vector ($0.86 \cdot 2\pi/a$ vs. $0.92 \cdot 2\pi/a$). We assign this difference to the fact that we used the LDA functional, while in Ref. [17] the PBE functional was employed [66].

IV. CONCLUSIONS

In conclusion, we described an implementation of time-dependent density-functional perturbation theory for spin fluctuations, based on plane waves and pseudopotentials, built around the linear response modules of the QUANTUM ESPRESSO package. In the present approach we calculate the macroscopic spin susceptibility $\chi(\mathbf{q},\omega)$ via a self-consistent solution of the time-dependent Sternheimer equation. The main advantage of this formulation is that it avoids altogether the need for evaluating unoccupied Kohn-Sham states.

We demonstrated the methodology by calculating spin wave spectra of bcc Fe, fcc Ni, and bcc Cr along several high-symmetry directions in the Brillouin zone, and we rationalized the suppression of magnon excitations in terms of Landau damping when the magnon energy resonates with the Stoner continuum. In the case of Fe and Ni, our calculated magnon dispersions relations are in good agreement with previous theoretical results near the zone center, but we see some significant deviations closer to the zone boundaries. These deviations likely result from the underlying DFT description of the ground-state electronic structure. In the case of Fe, our calculations are in reasonable agreement with experiment, while in the case of Ni the calculated magnon energies are too large by a factor of two. This discrepancy is consistent with previous *ab initio* calculations and is attributed to the fact that standard DFT yields too large a Stoner splitting for this metal as compared to experiment. In the case of Cr, we demonstrated that the calculation of spin wave spectra can be a very powerful tool to identify SDW phases, and we obtained good agreement with previous theory and with experiment.

Looking forward, we see two main avenues for future development. Firstly, it would be desirable to extend the present formalism and implementation to Hubbard-corrected DFT. The capability of calculating the spin susceptibility within DFT+U would make it possible to explore many interesting correlated electron systems, including for example the copper oxides high-temperature superconductors. Secondly, it would be important to incorporate support for spin-orbit coupling

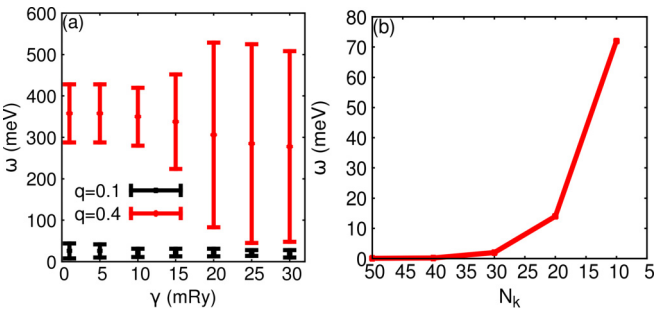

FIG. 4. (a) Calculated magnon energies of Ni together with full width at half maximum of corresponding magnon peaks. Wave vectors are given in units of $2\pi/a(1,0,0)q$. (b) Calculated magnon energies of Ni at $\mathbf{q} = (0,0,0)$ with respect to $\mathbf{k}$-points meshes used in the ground state calculations. The $\mathbf{k}$-points meshes are given in $N_k \times N_k \times N_k$. Linear response calculations are all performed with $50 \times 50 \times 50$ $\mathbf{k}$-points mesh.

in the methodology. This further development will enable calculations of spin wave spectra on systems with strong magnetic anisotropy, for example multiferroic oxides. Apart from these desirable improvements, we believe that our current implementation provides an important addition to state-of-the-art techniques for investigating spin fluctuations, magnon dispersions, and spin density waves in several important problems of condensed matter physics, and will serve as a starting point to explore incommensurate magnetic excitations systematically, without performing supercell calculations.

Note added. We are aware of a closely related work, where the authors used TD-DFPT to calculate magnon dispersion relations [67]. The present results are consistent with those of Ref. [67].

ACKNOWLEDGMENTS

This work was funded by EPSRC Grant No. EP/M020517/1, entitled "Oxford Quantum Materials Platform Grant" and the Leverhulme Trust (Grant No. RL-2012-001). The authors acknowledge the use of the University of Oxford Advanced Research Computing (ARC) facility (http://dx.doi.org/10.5281/zenodo.22558) and the ARCHER UK National Supercomputing Service.

APPENDIX A: CONVERGENCE WITH RESPECT TO γ

Our results shown in the main body of this paper are all well converged with respect to the parameter γ used to deal with fractional occupations in Sec. II. Here we illustrate the convergence with respect to γ using Ni as a representative example. In Fig. 4(a), we can see that magnon dispersion at $\mathbf{q} = (0.1,0,0)2\pi/a$ and $\mathbf{q} = (0.4,0,0)2\pi/a$ are well converged with $\gamma = 10$ mRy.

APPENDIX B: GOLDSTONE MODE

In a ferromagnet in the absence of spin-orbit coupling, excitation energy of the Goldstone mode (acoustic magnon at Γ point) should vanish. In our formalism, nonzero Goldstone mode (the so called "gap error") can arise if there is inconsis-

tency between the density from the ground state calculations and that from the response calculations, e.g., two different **k**-points meshes are used in these two calculations. This is illustrated in Fig. 4(b) using Ni as a representative example. We can see that the "gap" closes as the ground state **k**-points mesh approaches the one used in the response calculations. The "gap error" is avoided if the same set of parameters (**k**-points, smearing) is used for both ground state and response calculations. This scheme is employed throughout our calculations in the main body of this paper. In practice, the energy of the Goldstone mode is below the smallest energy for which we have performed our calculations, e.g., 0.1 meV in Fig. 4(b).

[1] T. Moriya, *Spin Fluctuations in Itinerant Electron Magnetism* (Springer-Verlag, Berlin, 1985).
[2] D. J. Scalapino, Rev. Mod. Phys. **84**, 1383 (2012).
[3] P. Monthoux, D. Pines, and G. G. Lonzarich, Nature (London) **450**, 1177 (2007).
[4] S. A. Wolf, D. D. Awschalom, R. A. Buhrman, J. M. Daughton, S. von Molnár, M. L. Roukes, A. Y. Chtchelkanova, and D. M. Treger, Science **294**, 1488 (2001).
[5] I. Žutić, J. Fabian, and S. Das Sarma, Rev. Mod. Phys. **76**, 323 (2004).
[6] A. Khitun, M. Bao, and K. L. Wang, J. Phys. D: Appl. Phys. **43**, 264005 (2010).
[7] A. Pimenov, A. A. Mukhin, V. Y. Ivanov, V. D. Travkin, A. M. Balbashov, and A. Loid, Nat. Phys. **2**, 97 (2006).
[8] J. Van Kranendonk and J. H. Van Vleck, Rev. Mod. Phys. **30**, 1 (1958).
[9] C. Kittel, *Introduction to Solid State Physics* (Wiley, New York, 2004).
[10] L. D. Landau, J. Phys. USSR **10**, 25 (1946).
[11] P. A. Buczek, Ph.D. thesis, Martin Luther Universität, Halle-Wittenberg, 2009.
[12] A. T. Costa, R. B. Muniz, and D. L. Mills, Phys. Rev. B **70**, 054406 (2004).
[13] S. V. Halilov, H. Eschrig, A. Y. Perlov, and P. M. Oppeneer, Phys. Rev. B **58**, 293 (1998).
[14] R. Gebauer and S. Baroni, Phys. Rev. B **61**, R6459 (2000).
[15] P. Buczek, A. Ernst, and L. M. Sandratskii, Phys. Rev. B **84**, 174418 (2011).
[16] E. K. U. Gross and W. Kohn, Phys. Rev. Lett. **55**, 2850 (1985).
[17] S. Y. Savrasov, Phys. Rev. Lett. **81**, 2570 (1998).
[18] B. Rousseau, A. Eiguren, and A. Bergara, Phys. Rev. B **85**, 054305 (2012).
[19] E. Runge and E. K. U. Gross, Phys. Rev. Lett. **52**, 997 (1984).
[20] U. von Barth and L. Hedin, J. Phys. C: Solid State Phys. **5**, 1629 (1972).
[21] J. Callaway and C. S. Wang, J. Phys. F: Met. Phys. **5**, 2119 (1975).
[22] N. Marzari, A. A. Mostofi, J. R. Yates, I. Souza, and D. Vanderbilt, Rev. Mod. Phys. **84**, 1419 (2012).
[23] H. F. Wilson, F. Gygi, and G. Galli, Phys. Rev. B **78**, 113303 (2008).
[24] H. F. Wilson, D. Lu, F. Gygi, and G. Galli, Phys. Rev. B **79**, 245106 (2009).
[25] F. Giustino, M. L. Cohen, and S. G. Louie, Phys. Rev. B **81**, 115105 (2010).
[26] P. Umari, G. Stenuit, and S. Baroni, Phys. Rev. B **81**, 115104 (2010).
[27] P. Umari, X. Qian, N. Marzari, G. Stenuit, L. Giacomazzi, and S. Baroni, Phys. Status Solidi B **248**, 527 (2011).
[28] H.-V. Nguyen, T. A. Pham, D. Rocca, and G. Galli, Phys. Rev. B **85**, 081101 (2012).
[29] H. Lambert and F. Giustino, Phys. Rev. B **88**, 075117 (2013).
[30] P. Giannozzi, S. Baroni, N. Bonini, M. Calandra, R. Car, C. Cavazzoni, D. Ceresoli, G. L. Chiarotti, M. Cococcioni, I. Dabo *et al.*, J. Phys.: Condens. Matter **21**, 395502 (2009).
[31] https://github.com/mmdg-oxford/magnon-dev.
[32] K. Karlsson and F. Aryasetiawan, J. Phys.: Condens. Matter **12**, 7617 (2000).
[33] E. Şaşıoğlu, A. Schindlmayr, C. Friedrich, F. Freimuth, and S. Blügel, Phys. Rev. B **81**, 054434 (2010).
[34] F. Giustino, *Materials Modelling using Density Functional Theory, Properties and Predictions* (Oxford University Press, Oxford, UK, 2014).
[35] R. M. Sternheimer, Phys. Rev. **96**, 951 (1954).
[36] S. Baroni, S. de Gironcoli, A. Dal Corso, and P. Giannozzi, Rev. Mod. Phys. **73**, 515 (2001).
[37] S. Y. Savrasov, Phys. Rev. Lett. **69**, 2819 (1992).
[38] X. Gonze, Phys. Rev. A **52**, 1096 (1995).
[39] X. Andrade, S. Botti, M. A. L. Marques, and A. Rubio, J. Chem. Phys. **126**, 184106 (2007).
[40] L. Reining, G. Onida, and R. W. Godby, Phys. Rev. B **56**, R4301 (1997).
[41] T. Izuyama, D.-J. Kim, and R. Kubo, J. Phys. Soc. Jpn. **18**, 1025 (1963).
[42] A. A. Quong and B. M. Klein, Phys. Rev. B **46**, 10734 (1992).
[43] M. Kawamura, Y. Gohda, and S. Tsuneyuki, Phys. Rev. B **89**, 094515 (2014).
[44] S. de Gironcoli, Phys. Rev. B **51**, 6773 (1995).
[45] L. M. Sandratskii, J. Phys.: Condens. Matter **3**, 8565 (1991).
[46] D. R. Hamann, M. Schlüter, and C. Chiang, Phys. Rev. Lett. **43**, 1494 (1979).
[47] D. Vanderbilt, Phys. Rev. B **41**, 7892 (1990).
[48] S. Ismail-Beigi, E. K. Chang, and S. G. Louie, Phys. Rev. Lett. **87**, 087402 (2001).
[49] C. J. Pickard and F. Mauri, Phys. Rev. Lett. **91**, 196401 (2003).
[50] D. A. H. Jacobs, IMA J. Number Anal. **6**, 447 (1986).
[51] D. D. Johnson, Phys. Rev. B **38**, 12807 (1988).
[52] J. P. Perdew and A. Zunger, Phys. Rev. B **23**, 5048 (1981).
[53] A. D. Corso, Comput. Mater. Sci. **95**, 337 (2014).
[54] S. Lounis, A. T. Costa, R. B. Muniz, and D. L. Mills, Phys. Rev. B **83**, 035109 (2011).
[55] C. K. Loong, J. M. Carpenter, J. W. Lynn, R. A. Robinson, and H. A. Mook, J. Appl. Phys. **55**, 1895 (1984).
[56] J. W. Lynn and H. A. Mook, Phys. Rev. B **23**, 198 (1981).
[57] H. A. Mook and D. M. Paul, Phys. Rev. Lett. **54**, 227 (1985).
[58] N. Marzari, D. Vanderbilt, A. De Vita, and M. C. Payne, Phys. Rev. Lett. **82**, 3296 (1999).
[59] R. Raue, H. Hopster, and R. Clauberg, Z. Phys. B - Condensed Matter **54**, 121 (1984).

[60] D. E. Eastman, F. J. Himpsel, and J. A. Knapp, Phys. Rev. Lett. **44**, 95 (1980).
[61] C. R. Fincher, G. Shirane, and S. A. Werner, Phys. Rev. Lett. **43**, 1441 (1979).
[62] A. W. Overhauser, Phys. Rev. **128**, 1437 (1962).
[63] W. M. Lomer, Proc. Phys. Soc. (London) **80**, 489 (1962).
[64] E. Fawcett, Rev. Mod. Phys. **60**, 209 (1988).
[65] R. Hafner, D. Spišák, R. Lorenz, and J. Hafner, Phys. Rev. B **65**, 184432 (2002).
[66] J. P. Perdew, K. Burke, and M. Ernzerhof, Phys. Rev. Lett. **77**, 3865 (1996).
[67] T. Gorni, Ph.D. thesis, SISSA-Scuola Internazionale Superiore di Studi Avanzati, Trieste, Italy, 2016, http://hdl.handle.net/20.500.11767/43342.